Proc. Lunar Sci. Conf. 6th (1975), p. 843–869.
Printed in the United States of America

Experimental modeling of the cooling history of Apollo 12 olivine basalts

C. H. DONALDSON,[1]* T. M. USSELMAN,[2] R. J. WILLIAMS,[2] and G. E. LOFGREN[2]

[1]The Lunar Science Institute, 3303 NASA Rd. 1, Houston, Texas 77058

[2]NASA Johnson Space Center, Houston, Texas 77058

Abstract—An analog of the Apollo 12 olivine vitrophyres has been crystallized in a 1-atm gas-mixing furnace at cooling rates ranging between 1250 and 0.7°/hr and isothermally at degrees of supercooling ranging from 10°C to 325°C. Mineral chemistry, crystal shapes, grain sizes and textures are systematically related to cooling rate and degree of supercooling. At linear cooling rates ≤40°/hr the texture is porphyritic—large olivine crystals are set in a groundmass of finer-grained pyroxene, plagioclase, and ilmenite; a later generation of olivine never crystallizes. There are three shapes of olivine crystals in the Apollo 12 olivine vitrophyres, glomerocrysts of subhedral crystals, large subequant skeletons and highly elongate skeletons. These result from three generations of nucleation and a two-stage cooling history—a slow pre-eruption stage and a rapid, continuously increasing, post-eruption stage. During the post-eruption stage, the olivine vitrophyres cooled at rates which increased from 10°/hr to at least 100°/hr, whereas the olivine basalts cooled at rates <15°/hr, and the olivine gabbros at rates <2.7°/hr. It seems likely that the Apollo 12 olivine basalt magmas were erupted with olivine crystals in suspension.

The nucleation temperature of olivine in cooling rate experiments is dependent on the experimental technique, and hence, results of cooling experiments should be applied with caution.

INTRODUCTION

ROCKS OF THE OLIVINE BASALT GROUP of Apollo 12 mare basalts consist of porphyritic vitrophyres, basalts, and gabbros (Warner, 1971; James and Wright, 1972) in which olivine phenocrysts are set in finer-grained matrices. The porphyritic texture precludes unequivocal acceptance of these rocks as liquid compositions, because enrichment in crystals may have occurred, and prevents distinction between single- or multiple-stage cooling histories.

As part of a project examining the cooling, crystallization and emplacement of mare basalt flows (Lofgren *et al.*, 1974, 1975, this volume; Usselman *et al.*, 1975), a synthetic analog of an Apollo 12 olivine basalt has been crystallized at controlled cooling rates and degrees of supercooling. This paper describes the results of these experiments and, by comparison of the textures and mineral chemistries of run products with those of the natural olivine basalts, cooling rates are estimated for the Apollo 12 olivine basalts.

*Present address: Department of Geology, University of Manchester, Manchester Ml3 9PL, England.

The composition investigated resembles olivine vitrophyre 12009, a possible parental liquid composition of the Apollo 12 olivine basalts (Green *et al.*, 1971). In sample 12009 phenocrysts and glomerocrysts of olivine are set in a matrix of skeletal olivine, skeletal augite, and cryptocrystalline material. The experiments have application to crystallization of all the olivine basalts, but especially to the vitrophyres (samples 12009 and 12008) which are unique among the Apollo 12 basalts in having olivine crystals of three grain sizes and shapes (see later). If this trichotomy of olivine crystals can be produced under single-stage cooling conditions [cf. the two generations of pyroxene in the Apollo 15 quartz-normative basalts (Lofgren *et al.*, 1974)], then sample 12009 indeed may have been a liquid. As part of this study, the compositions of phases in sample 12009 have been determined, to augment the work of Brett *et al.* (1971) and Butler (1972).

A similar investigation has been made by Walker *et al.* (1975) of holocrystalline olivine basalt 12002. Certain results of the present study differ significantly from those of Walker *et al.* (1975).

EXPERIMENTAL

Crystallization experiments were performed in a CO–CO_2 gas-mixing furnace using the platinum wire-loop technique (Donaldson *et al.*, 1975) to support the sample. Charges were melted for 2 hr, 20–30°C above the liquidus temperature of the material (Fig. 1) and at $f_{O_2} = 10^{-11.1}$–$10^{-11.2}$ atm [cf. $10^{-11.8}$ atm, the intrinsic liquidus f_{O_2} of sample 12009 (Sato, 1973)]. The furnace was then either (1) rapidly cooled (at approximately 2500°/hr) to a crystallization isotherm which was maintained for approximately 20 hr before quenching, or (2) cooled at a controlled rate to approximately the solidus temperature and then quenched. Types of cooling behavior investigated were linear rates, two-stage cooling, log temperature proportional to log time and temperature proportional to log time. Summaries of the cooling rate experiments and the isothermal supercooling experiments are shown in Tables 1a and 1b. In all experiments, the ratio of CO_2:CO in the gas atmosphere (set at the liquidus temperature to be 10^{-11} atm of oxygen) was not altered during experiments and the f_{O_2} therefore decreases on cooling. Approximate values of f_{O_2} at various run temperatures are shown in Fig. 1.

Thin sections of the charges were prepared for petrographic study and chemical analysis of phases. Analyses were made on an ARL-EMX-SM electron microprobe, using a 1–2-μ diameter electron beam, a beam current of 0.02 microamps and an accelerating potential of 15 kV. Analyses were corrected for deadtime, background, instrument drift, and matrix effects.

The fused-glass analog of sample 12009 (Table 2) is depleted in Fe and enriched in Al relative to the natural rock. These differences decrease the content of mafic minerals and increase that of plagioclase relative to the natural rock. They also expand the spinel stability field.

The equilibrium phase relations of the analog are compared in Fig. 1 with those determined for 12009 by Green *et al.* (1971), who ran experiments in iron capsules sealed in evacuated silica tubes. The f_{O_2} in the present experiments is always less than the iron–wüstite buffer curve and, on cooling, decreases more rapidly than that in experiments run in iron capsules. The differences between the phase relations of the analog and sample 12009 are consistent with the bulk composition difference between the materials. Specifically, the natural sample and its olivine are more Fe-rich.

MORPHOLOGIC VARIATION

Olivine. Olivine crystals show the same systematic change in shapes with increasing cooling rate as with degree of supercooling (Donaldson, in prepara-

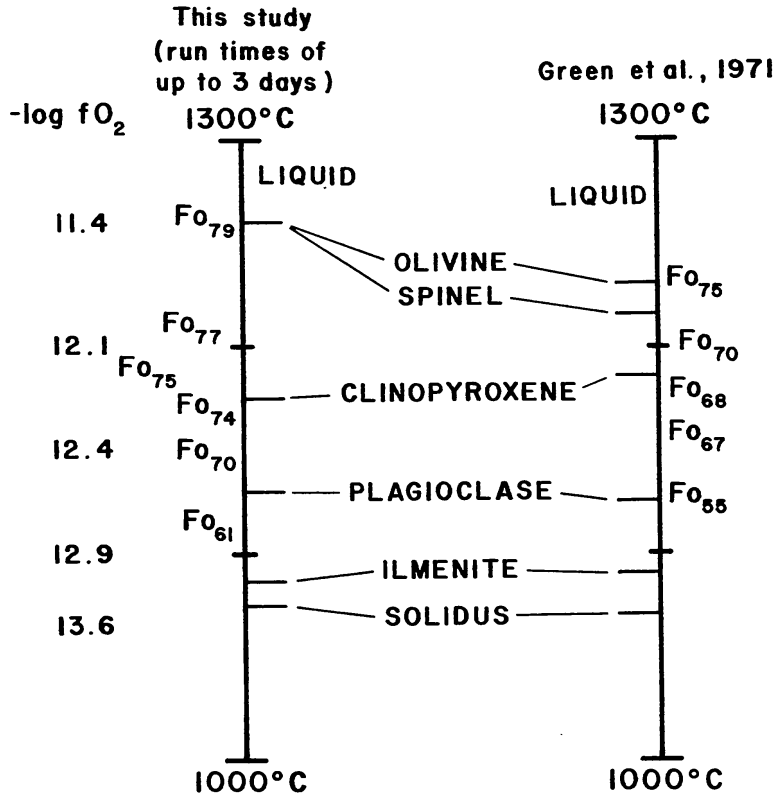

Fig. 1. Phase relations of 12009 analog compared to sample 12009. The oxygen fugacity of the present experiments is shown on the left at various temperatures. The olivine compositions at various isotherms are also compared.

Table 1a. Run conditions of cooling rate experiments.

	Run no.	Cooling rate °C/hr	Comments	Finish T°C	Finish $-\log_{10} f_{O_2}$
	C16	1430		1080	14.1
	C15	650		1090	13.6
	C14	380		1100	13.6
Linear	C13	168		1090	13.1
cooling	C17	86		1080	13.7
	C12	40		1095	13.7
	C10	15.5		1090	14.3
	C11	7.2		1090	14.1
	C27	2.7		1047	14.2
Two-stage	C28	3→200	Cooling rate	1050	14.3
cooling	C29	1.5→70	increased at	1050	13.8
	C30	4→35	1200°C	1060	14.2
Continuously			Cooling path of		
decreasing	C31	13→0.9	form $\Delta T \propto \log t$	988	15.5
cooling rate	C32	22→0.7	Cooling path of form $\log \Delta T \propto \log t$	1010	14.9

Table 1b. Run conditions of isothermal supercooling experiments.

Run no.	Temperature °C	Supercooling (ΔT) °C	$-\log_{10} f_{O_2}$
C24	1250	10	11.3
C23	1232	28	11.7
C18	1203	55	12.0
C9	1190	71	12.6
C25	1180	81	12.0
C19	1150	111	12.7
C21	1110	150	13.0
C26	1058	202	13.3
C8	935	325	16.6

tion). Subhedral olivines crystallize at the slowest cooling rates and smallest degrees of supercooling (Tables 3 and 4). As the values of these parameters increase, the shapes progress from subequant, externally euhedral but internally skeletal crystals, through hollow skeletons, to elongate, internally and externally skeletal crystals, to chain-like forms, to lattice-work forms, to dendrites (Tables 3 and 4).

Pyroxene. The shapes of pyroxene crystals change with increasing supercooling and cooling rate from subequant, subhedral grains, through elongate subhedral

Table 2. Composition of starting material[1] compared with sample 12009.

	Starting material[2]	Sample 12009[3]
SiO_2	45.83	45.03
TiO_2	2.85	2.90
Al_2O_3	10.44	8.59
Cr_2O_3	0.37	0.55
FeO	16.20	21.03
MnO	0.27	0.28
MgO	11.65	11.55
CaO	11.82	9.42
Na_2O	0.26	0.23
Total	99.74	99.58
MgO/MgO + FeO wt. ratio	0.42	0.35

[1]Sample provided by C. H. Simonds.

[2]Electron microprobe analyses of glass charge melted at 20°C above the liquidus for 2 hr.

[3]Analysis by Compston *et al.* (1971).

Table 3. Crystal morphology as a function of cooling rate.

Cooling rate °C/hr	Olivine	Pyroxene	Plagioclase	Opaques
1400	Dendrites with 1^{y}, 2^{y}, 3^{y}, and 4^{y} branching (Fig. 2a)	None	None	None
650	Thinly tabular, parallel growths of lattice-work and chain-like shape (Fig. 2b)	Curved dendrites and spherulites (Fig. 2b)		Euhedral octahedra of chromite
380	Randomly oriented lattice-work and chain-like shapes (Fig. 2c)	(Fig. 2c)		
170	↓	None		
86	Randomly oriented chain-like shapes (Fig. 2d)	Curved dendrites and elongate chain-like skeletons (Fig. 2d)		
40	Elongate, internally and externally skeletal crystals (Fig. 2e)	(Fig. 2e)		
15	Elongate and subequant, euhedral, hollow skeletons (Fig. 2f)	Elongate, curved, subhedral grains, and elongate chain-like skeletons (Fig. 2g)	Elongate skeletal laths	Euhedral octahedra of chromite and anhedral grains of ilmenite
7	Subequant, euhedral, internally skeletal crystals (Fig. 2h)	Subhedral, subequant grains (Fig. 2i)		
2.7	↓			

Table 4. Crystal morphology as a function of supercooling.

Supercooling °C	Olivine	Pyroxene	Plagioclase	Opaques
325	None	None	None	None
200	↓	↓	↓	↓
150	Chainlike	Elongate curved grains and spherulites	Elongate skeletons	Euhedral octahedra of chromite
110	(Fig. 2j)	Subequant, subhedral grains (Fig. 2j)	None	(Fig. 2j)
80		None		
70	Elongate, internally and externally skeletal crystals			
55	Elongate, externally skeletal crystals			
28				
10				

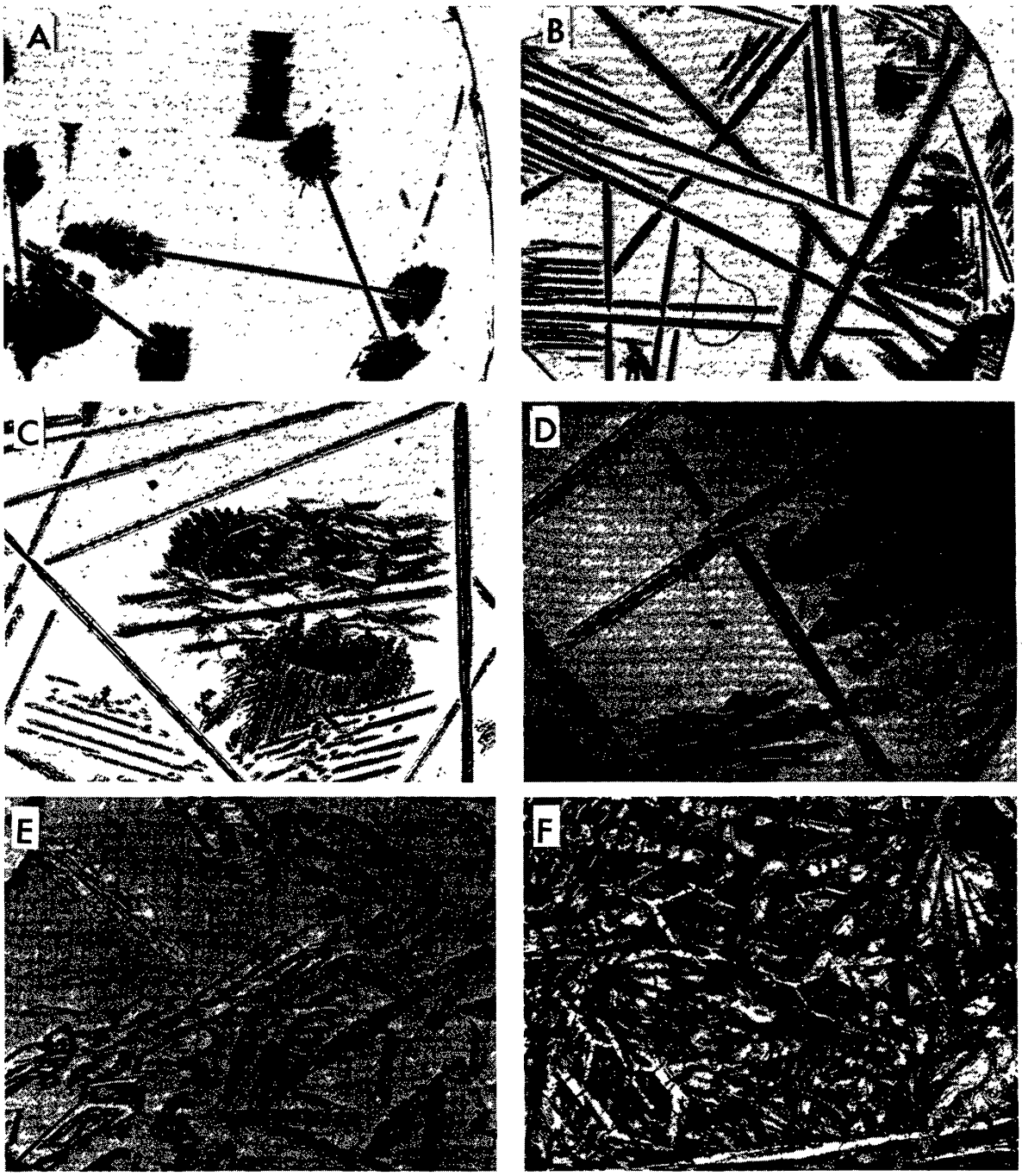

Fig. 2. Photomicrographs of crystal morphologies and textures of run products (field of view given in brackets): (a) 1430°/hr (4 mm); (b) 650°/hr (4.5 mm); (c) 380°/hr (2.5 mm); (d) 86°/hr (2 mm); (e) 40°/hr (1.8 mm); (f) 15.5°/hr (3 mm);

grains, to elongate curved grains, to elongate grains with skeletal chain-like form, to curved dendrites, to spherulites (Tables 3 and 4). There is a systematic decrease in elongation and grain size of the pyroxene with decreasing cooling rate and degree of supercooling.

Plagioclase. Narrow, acicular, cored skeletons of plagioclase grew in two cooling rate runs and one supercooling run. That plagioclase nucleation is a

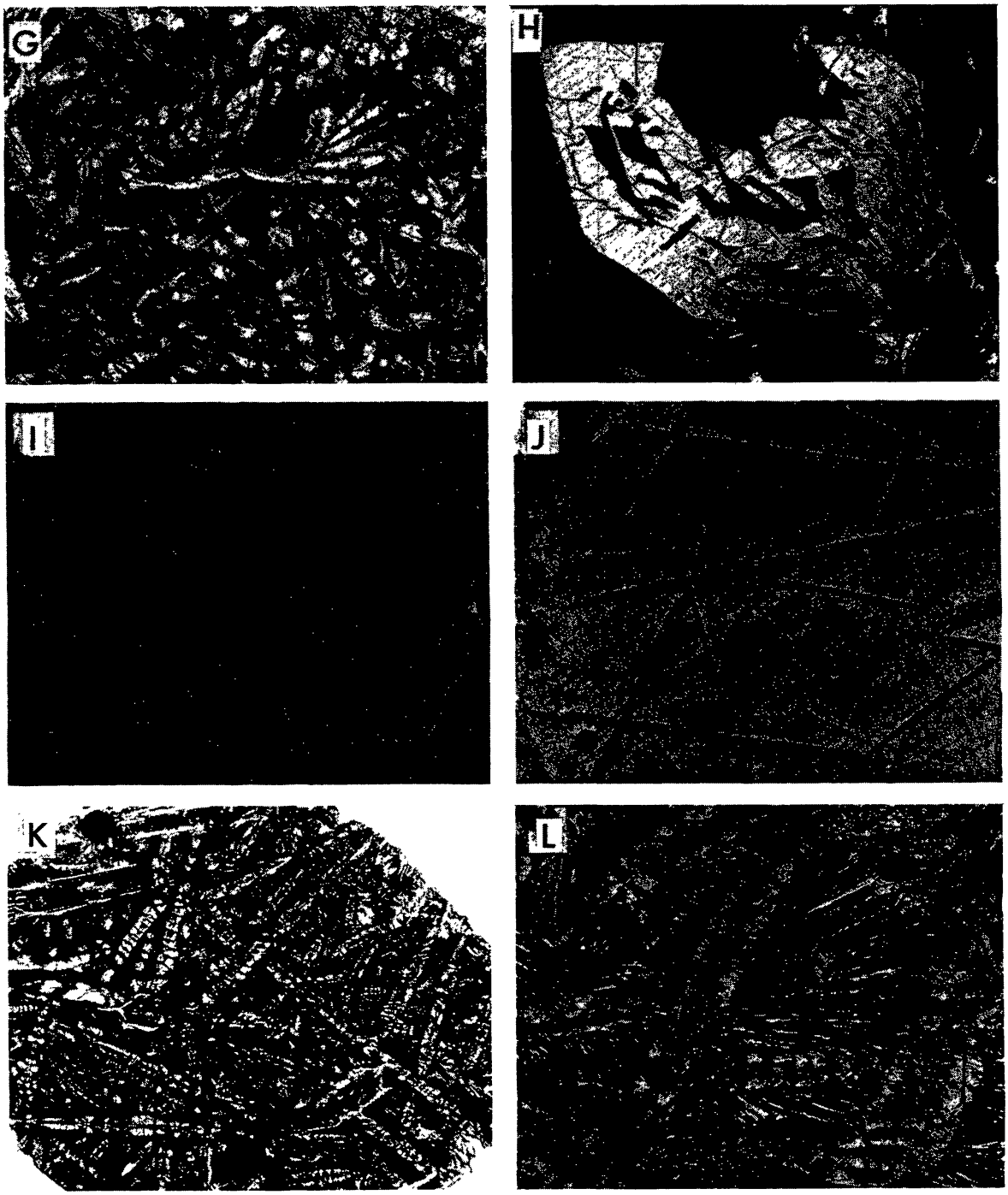

Fig. 2. (*Continued*) Photomicrographs of crystal morphologies and textures of run products (field of view given in brackets): (g) 15.5°/hr (0.9 mm); (h) 7.2°/hr (1 mm); (i) 7.2°/hr (0.8 mm); (j) 1149°C (4 mm); (k) log $T \propto \log t$ (6 mm); (l) log $T \propto \log t$ (1.2 mm).

chance event is demonstrated by the presence of plagioclase in one charge cooled at 2.7°/hr and its absence in another charge cooled at the same rate.

Opaques. The shape and size of the small, euhedral grains of chromite are unrelated to the cooling rate or the degree of supercooling of the melt. Chromite dendrites were not observed, even in very rapid cooling runs (contrast Lofgren *et*

al., 1974). Ilmenite crystallized only in the 2.7°/hr, the 7°/hr and the nonlinear cooling runs. In the first and last of these runs it forms large anhedral crystals in the intersertal patches between plagioclase and pyroxene crystals, whereas in the 7°/hr run ilmenite forms minute, anhedral blebs in residual glass.

Textural Variations and Paragenesis

All the run products are hemicrystalline, with glass contents ranging from 5 to 80 vol.%. They vary from medium-grained to fine-grained; the faster-cooled runs are not necessarily the finest grained. Olivine crystals grow up to 6 mm in length, pyroxenes up to 3.5 mm, and plagioclase up to 1 mm.

At all cooling rates investigated, olivine crystals are larger than pyroxene, and the texture is porphyritic. At cooling rates $>15 < 650$°/hr olivine and pyroxene crystals are set in random orientation in glass. The texture is best described as porphyritic-intersertal. With decreasing cooling rate both minerals decrease in grain size. At cooling rates <15°/hr pyroxene forms discrete granules (Fig. 2i) between plagioclase laths and olivine phenocrysts (Fig. 2h), resulting in an olivine porphyry with intergranular matrix texture.

In isothermal runs, the olivine and pyroxene crystals are generally of comparable size. However, in a run at 1110°C, skeletal olivines set in a much finer-grained groundmass of plagioclase and pyroxene indicate that porphyritic texture can form under isothermal conditions.

Under no conditions did a porphyritic texture with two generations of olivine crystals develop. Neither did seriate textures form.

In the log temperature (T) versus log time (t) and temperature versus log time experiments, the cooling rates over the first 100° are approximately 22 and 13°/hr respectively. The olivine and pyroxene crystals adopt shapes and sizes identical to those in the linear cooling experiment at 15.5°/hr. The very slow cooling (~0.8°/hr) at completion of these nonlinear cooling paths causes more extensive crystallization of the charges compared to the linear paths, and also promotes crystallization of the groundmass crystals. In both runs the texture is porphyritic with large skeletal olivines and elongate pyroxenes set in a groundmass of finer-grained plagioclase and ilmenite (Fig. 2k). The groundmass texture of the $\log T \propto \log t$ run is radiate (Fig. 2l), that of the $\log t \propto T$ run is subophitic to intrafasciculate (Drever *et al.*, 1972). The pyroxene between plagioclase laths in the former run is not a second generation, but is continuous with the early formed pyroxene crystals; a second pyroxene generation is present in the $\log t \propto T$ run.

In runs containing both plagioclase and pyroxene, plagioclase crystals abut onto pyroxene and are enclosed by glass, never by pyroxene. These textural relations reflect the late-stage crystallization of plagioclase in the paragenetic sequence (Fig. 1), and the suppression of its nucleation with cooling (Gibb, 1974; Walker *et al.*, 1975).

In cooling runs, chromite is consistently set in glass or is enclosed by olivine. It is never enclosed by pyroxene. The former relation indicates nucleation of chromite before olivine and the latter relation would traditionally be interpreted to

indicate crystallization of pyroxene before chromite. Since olivine always crystallizes before pyroxene from this melt (Fig. 1), an alternative interpretation is required. It seems that before nucleation of pyroxene, most of the chromite not enclosed by olivine has settled to the base of the charge. This suggestion is consistent with the preferred location of chromite crystals at the base of the charge.

It is noticeable that ilmenite appears only in runs containing plagioclase, suggesting that crystallization of olivine and pyroxene alone does not enrich the residual melt sufficiently in Fe and Ti for saturation with ilmenite.

Some of the cooling runs contain sparse 1–3-μ beads of metallic iron. These are consistently enclosed only by glass and are considered very late-stage crystallization products.

PHASE CHEMISTRY

Olivine. Core compositions of olivine in cooling rate runs range between $Fo_{78.6}$ and Fo_{71}. The extent of normal zoning is not systematically related to the cooling rate (Table 5); however, as the cooling rate increases, the core composition becomes progressively more Fe-rich, indicating that the nucleation temperature of olivine is suppressed with increasing cooling rate. The compositions of olivines grown in the isothermal experiments define the olivine solidus of the melt used. The core compositions of olivines in cooling rate runs compared with those grown in isothermal runs therefore yield an estimate of the nucleation temperature of olivine in the cooling rate experiments (Fig. 3); for example, olivine grown during cooling at 86°/hr nucleated at 1195°C (Fig. 3). The comparison assumes that the olivines nucleating in the cooling rate experiments have identical composition to

Table 5. Analyses of synthetic olivines formed at different cooling rates and

Cooling rate or temperature	1430°/hr	650°/hr	380°/hr	86°/hr rim	86°/hr core	40°/hr rim	40°/hr core	15.5°/hr rim	15.5°/hr core	7°/hr rim	7°/hr core	2.7°/hr core
SiO_2	37.67	38.00	37.26	36.90	37.47	37·69	38.24	38.62	39.29	37.41	37.86	38.25
TiO_2	0.20	0.11	0.09	0.10	0.14	0.09	0.07	0.07	0.04	0.06	0.07	0.04
Cr_2O_3	0.38	0.19	0.29	0.33	0.36	0.27	0.28	0.29	0.28	0.25	0.27	0.18
FeO	25.09	24.17	23.65	24.05	22.11	25.11	21.07	25.56	19.62	22.72	20.00	19.86
MnO	0.32	0.33	0.32	0.35	0.32	0.34	0.30	0.34	0.33	0.35	0.29	0.28
MgO	35.44	37.04	36.87	37.64	39.56	36.08	39.27	35.58	40.43	38.07	40.29	40.68
CaO	0.60	1.12	0.44	0.51	0.42	0.39	0.34	0.44	0.36	0.42	0.31	0.40
Total	99.70	100.96	98.92	99.88	100.38	99.97	99.57	100.90	100.35	99.28	99.09	99.69
Si	0.999	0.997	0.990	0.975	0.975	0.996	0.995	1.011	1.055	0.986	0.987	0.988
Ti	0.004	0.002	0.002	0.002	0.003	0.002	0.001	0.001	0.001	0.001	0.001	0.001
Cr^{3+}	0.008	0.004	0.006	0.007	0.007	0.006	0.006	0.006	0.006	0.005	0.005	0.004
Fe	0.556	0.524	0.526	0.531	0.481	0.555	0.459	0.559	0.420	0.501	0.436	0.429
Mn	0.007	0.007	0.007	0.008	0.007	0.008	0.007	0.007	0.007	0.008	0.006	0.009
Mg	1.401	1.431	1.461	1.482	1.534	1.422	1.523	1.388	1.542	1.496	1.565	1.572
Ca	0.001	0.03	0.012	0.014	0.012	0.001	0.009	0.012	0.010	0.01	0.009	0.011
Fo mol.%	71.3	72.9	73.3	73.3	75.9	71.6	76.6	71.03	78.3	74.6	78.0	78.6

[1]See text for description of different olivine types.

those grown in the isothermal crystallization experiments at the same isotherms. Hopper and Uhlmann (1974) have shown theoretically that this need not be true. However, the crystallization of *homogeneous* olivines in the isothermal supercooling experiments supports our assumption. The inferred nucleation temperatures are probably within ±10°C of the actual values.

The olivine incorporates more Ca, Ti, and Cr with increasing cooling rate. In isothermal experiments the Ca and Ti contents increase with supercooling, whereas the Cr content remains essentially constant (Table 5).

Pyroxene. In contrast to pyroxenes in lunar rocks, the extent of zoning in the laboratory-grown crystals is small (Table 6). The extremely Fe-enriched pyroxenes found in most mare basalts did not crystallize (Fig. 4). All the pyroxene is augite, which is continuously zoned from a less calcic core to a more calcic rim (Fig. 4). The zoning trends are consistently convex toward the En–Wo join, reflecting the more rapid enrichment of the pyroxene in Wo relative to Fs. With increasing cooling rate, the Fe/Fe + Mg ratio of pyroxenes systematically increases for a given Wo content, suggesting that pyroxenes in the faster-cooled runs nucleated at lower temperature. Comparison of the compositions of pyroxenes grown in cooling rate and isothermal runs indicates that crystals in the run cooled at 7°/hr nucleated at less than 1150°C; those in the 650°/hr run nucleated below 1110°C. The Wo content of the core compositions of crystals also changes with cooling rate (Fig. 4): crystals grown at 40 and 86°/hr contain up to 6 mol.% less Wo than those grown at ≤15°/hr and at 650°/hr. The cause of this minimum in Wo content is unknown.

More Cr, Al, and Ti are incorporated into the pyroxene at faster cooling rates; at greater supercooling, more Al and Ti enter the pyroxene, whereas Cr content is

different degrees of supercooling and compared with olivines in sample 12009.

						Natural olivines from sample 12009			
1110°C	1150°C	1180°C	1190°C	1203°C	1250°C	Type I[1] core	Type II core	Type III core	Type III rim
36.16	37.20	38.31	38.20	38.15	37.84	38.23	37.22	37.08	35.39
0.15	0.13	0.08	0.08	0.06	0.04	0.04	0.06	0.08	0.11
0.20	0.24	0.28	0.24	0.22	0.20	0.36	0.37	0.36	0.25
33.68	26.79	23.52	21.88	21.15	19.94	21.97	26.45	27.83	36.25
0.40	0.40	0.32	0.35	0.26	0.23	0.25	0.31	0.32	0.39
29.61	35.42	37.73	38.27	39.79	40.33	38.58	35.02	33.68	26.87
0.47	0.49	0.43	0.41	0.45	0.41	0.19	0.31	0.33	0.41
100.67	100.67	100.67	99.43	100.08	98.99	99.62	99.74	99.68	99.67
0.991	0.982	0.997	1.000	0.988	0.986	0.999	0.995	0.998	0.997
0.003	0.003	0.002	0.002	0.001	0.001	0.001	0.001	0.002	0.002
0.004	0.006	0.006	0.005	0.005	0.005	0.007	0.008	0.008	0.006
0.772	0.592	0.512	0.479	0.457	0.432	0.480	0.591	0.627	0.854
0.009	0.009	0.007	0.008	0.006	0.006	0.006	0.007	0.007	0.010
1.209	1.395	1.463	1.492	1.536	1.572	1.503	1.396	1.352	1.128
0.014	0.014	0.012	0.011	0.013	0.011	0.005	0.009	0.009	0.012
60.8	70.2	73.8	75.4	76.8	78.4	75.8	70.3	68.3	56.9

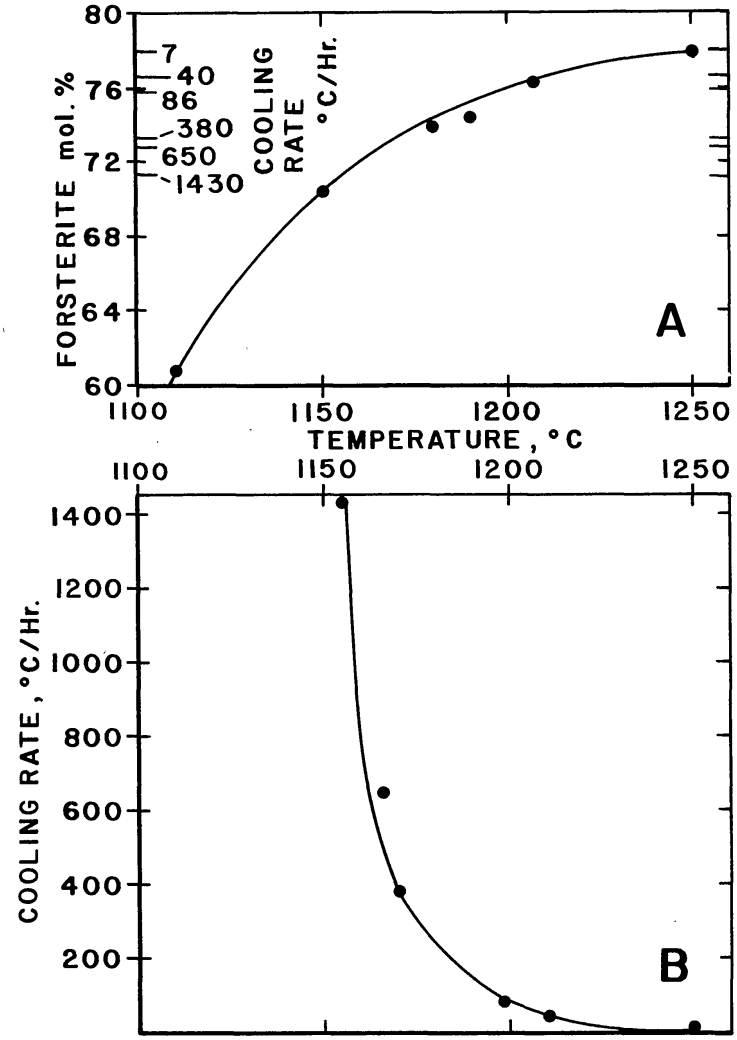

Fig. 3. Relation of olivine composition to crystallization temperature and cooling rate. (a) Olivine solidus defined by temperature-composition data for isothermal runs. The compositions of the olivine cores in each cooling rate experiment are shown on the ordinate. (b) Nucleation temperature of olivine as a function of cooling rate. (Constructed from Fig. 3a by estimating the temperature of an isothermal run at which olivine of the same composition as cores in each cooling rate experiment would grow.)

apparently insensitive to the degree of supercooling. In relative abundance of Cr, Al, and Ti, pyroxenes are typically zoned from Al^{VI}-rich cores to Ti-rich rims (Fig. 5). Cr content is essentially constant. Note that the pyroxenes grown in isothermal runs are zoned with respect to Al and Ti, possibly reflecting the relative times of nucleation of each crystal analyzed (and hence, the composition of the melt at that time), and the differences in growth rate of each crystal face. The more Cr-rich pyroxenes in the 1150°C run are attributable to crystallization in the absence of chromite.

The ratio of Ti:Al ions is typically less than 1:4 (Fig. 6). As cooling rate and degree of supercooling decrease, the Al and Ti contents systematically diminish. Individual crystals zone from Al- and Ti-deficient cores to Al- and Ti-rich rims. In the 7°/hr run, one pyroxene in a charge containing plagioclase has a rim containing Ti and Al in the ratio of approximately 1:2 (Fig. 6).

Table 6. Pyroxene analyses.

Cooling rate or temperature	650°/hr	380°/hr core	380°/hr rim	86°/hr core	86°/hr rim	40°/hr core	40°/hr rim	15.5°/hr core	15.5°/hr rim	7°/hr core	7°/hr rim	1110°C	1150°C	Natural pyroxene in sample 12009 core → rim			
SiO_2	45.73	47.92	46.92	48.63	47.53	48.76	49.52	48.87	48.68	50.32	48.81	47.73	49.46	50.89	46.07	42.59	46.68
TiO_2	2.63	1.92	3.06	1.96	2.32	1.63	1.94	2.17	1.85	1.60	2.27	1.52	1.36	0.95	2.34	5.35	4.03
Al_2O_3	7.25	7.27	7.73	7.34	7.13	6.85	6.08	6.21	5.67	4.38	6.79	6.52	4.05	2.71	6.21	9.32	5.72
Cr_2O_3	1.35	1.26	1.17	1.12	1.43	1.26	1.45	1.15	0.90	0.56	0.98	0.99	1.14	1.18	1.55	0.24	0.14
FeO	9.79	11.45	10.71	11.38	10.48	10.11	8.82	9.23	8.53	10.16	8.43	10.47	8.39	17.21	13.47	14.04	24.75
MnO	0.28	0.26	0.24	0.29	0.26	0.29	0.29	0.25	0.28	0.26	0.22	0.22	0.23	0.30	0.26	0.25	0.32
MgO	12.34	15.55	13.51	17.01	15.45	18.42	15.55	15.11	14.16	15.79	13.96	13.21	16.56	22.35	13.92	9.36	5.05
CaO	18.97	14.62	17.45	12.68	16.04	13.51	16.82	16.79	19.58	17.11	18.88	18.60	17.95	3.96	14.44	17.97	12.27
Na_2O	0.05	0.04	0.05	0.04	0.05	0.03	0.05	0.04	0.04	0.04	0.05	0.04	0.04	0.02	0.04	0.05	0.04
Total	98.39	100.29	100.84	100.45	100.69	100.86	100.52	99.65	99.69	100.22	100.39	99.30	99.18	99.57	98.30	99.17	99.00
Si	1.751	1.777	1.743	1.787	1.761	1.781	1.820	1.812	1.817	1.863	1.802	1.800	1.847	1.889	1.770	1.647	1.863
Ti	0.076	0.054	0.085	0.054	0.064	0.045	0.054	0.060	0.052	0.044	0.063	0.043	0.038	0.027	0.068	0.156	0.121
Al	0.327	0.318	0.338	0.318	0.309	0.295	0.263	0.271	0.249	0.191	0.295	0.290	0.178	0.118	0.281	0.425	0.264
Cr	0.041	0.037	0.034	0.032	0.042	0.036	0.042	0.034	0.027	0.016	0.029	0.030	0.034	0.035	0.047	0.007	0.005
Fe	0.314	0.355	0.333	0.350	0.322	0.309	0.271	0.286	0.266	0.315	0.260	0.330	0.262	0.534	0.433	0.454	0.826
Mn	0.009	0.008	0.008	0.009	0.008	0.009	0.009	0.008	0.009	0.008	0.007	0.007	0.007	0.009	0.008	0.008	0.011
Mg	0.693	0.860	0.748	0.932	0.857	1.003	0.851	0.835	0.788	0.871	0.768	0.743	0.922	1.237	0.797	0.539	0.301
Ca	0.778	0.581	0.695	0.499	0.635	0.529	0.662	0.667	0.783	0.679	0.747	0.752	0.718	0.158	0.594	0.744	0.525
Na	0.004	0.003	0.003	0.003	0.003	0.002	0.004	0.003	0.003	0.003	0.004	0.003	0.003	0.002	0.003	0.004	0.003
Wo	43.4	32.2	38.9	27.9	34.9	28.6	36.9	37.2	42.4	36.3	41.9	41.0	37.6	8.2	32.6	42.8	31.8
En	38.6	47.7	41.9	52.1	47.0	54.2	47.5	46.6	42.6	46.5	43.1	40.6	48.3	64.1	43.7	31.0	18.2
Fs	18.0	20.1	19.2	20.0	18.1	17.2	15.6	16.0	15.0	17.2	15.0	18.4	14.09	27.7	23.7	26.2	50.0

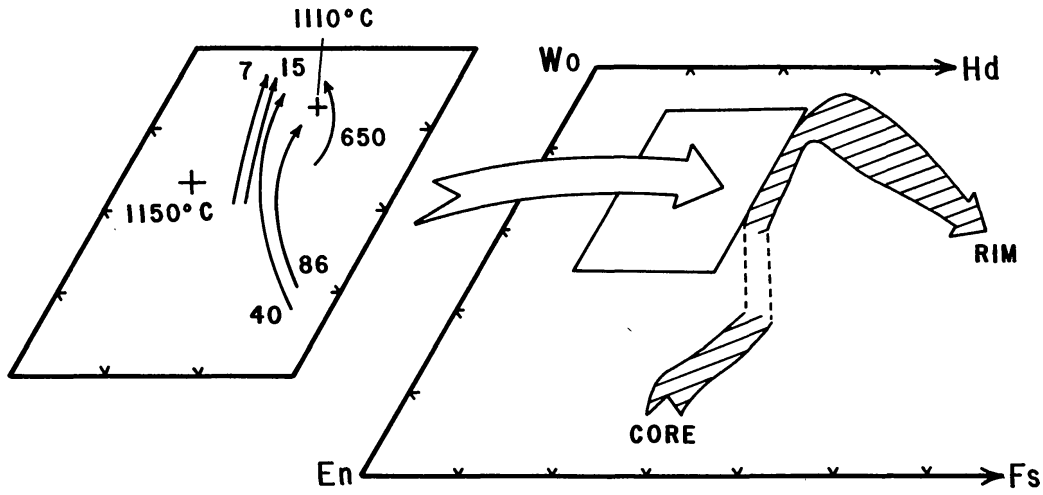

Fig. 4. Summary of pyroxene compositions. Arrows point from core to rim of crystals; numbers without units are cooling rates in °/hr; the two crosses are isothermal experiments. Hachured area is range of pyroxene composition in sample 12009 (data from this study).

Plagioclase. The three cooling rate runs which contain plagioclase exhibit a systematic decrease in anorthite content (and hence nucleation temperature) of crystals with increasing cooling rate (Table 7). Accompanying this variation are systematic increases in the Fe and Mg contents. Comparison of the compositions in the cooling rate runs with that of plagioclase in the only plagioclase-bearing

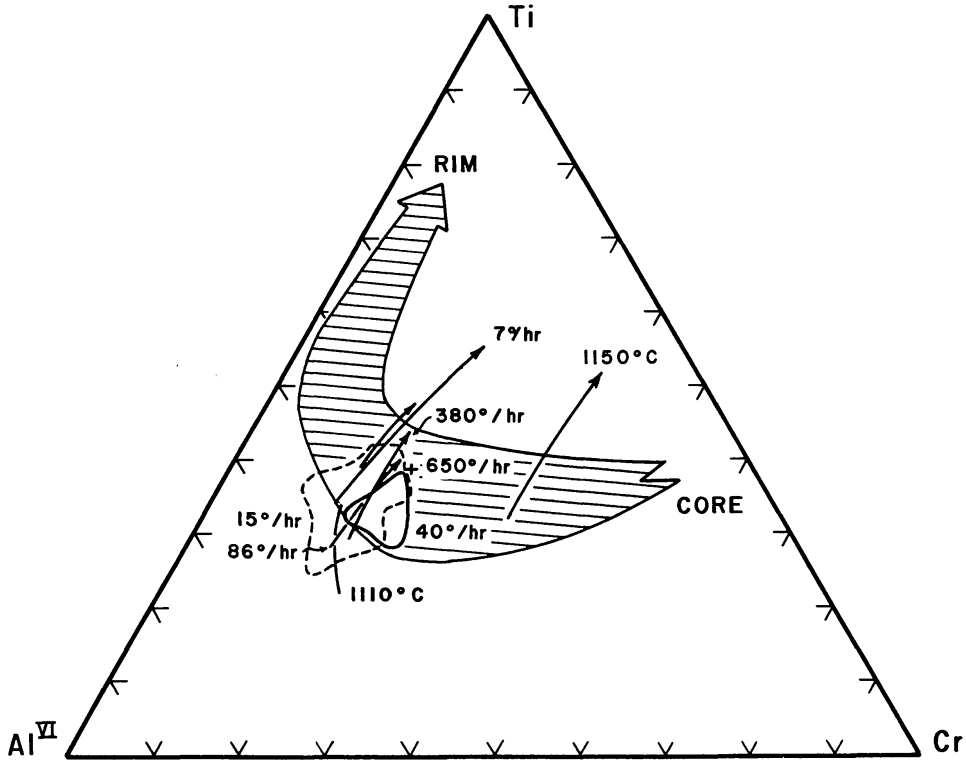

Fig. 5. Ti–Cr–Al^{VI} relations of pyroxenes (atomic proportions). Arrows point toward margin of crystals. Hachured area is for pyroxenes in sample 12009.

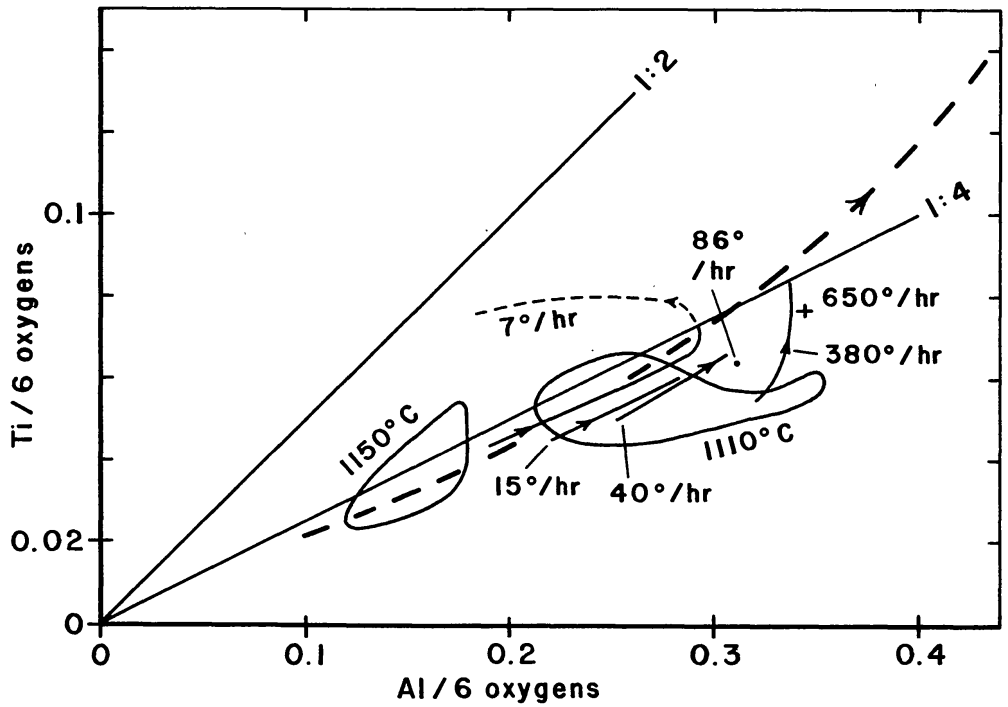

Fig. 6. Ti–Al relations of pyroxenes. Arrows point from core to rim of crystals. Heavy dashed line is trend of compositions in sample 12009.

Table 7. Plagioclase analyses.

Cooling rate or temperature		2.5°/hr	7°/hr	15.5°/hr	1110°C
SiO_2		48.66	48.53	49.27	47.41
TiO_2		0.17	0.14	0.19	0.11
Al_2O_3		30.80	31.34	30.42	32.49
FeO		1.08	1.21	1.54	0.93
MnO		0.02	0.02	0.03	0.02
MgO		0.63	0.66	0.74	0.47
CaO		17.24	17.30	16.92	17.52
Na_2O		0.70	0.88	1.02	0.96
K_2O		0.03	0.04	0.06	0.03
Total		99.33	100.12	100.19	99.94
Si		2.249	2.217	2.263	2.184
Ti		0.006	0.005	0.007	0.004
Al		1.678	1.734	1.647	1.764
Fe		0.042	0.047	0.059	0.036
Mn		0.001	0.001	0.001	0.001
Mg		0.043	0.046	0.051	0.032
Ca		0.854	0.847	0.833	0.865
Na		0.063	0.078	0.091	0.086
K		0.002	0.002	0.004	0.002
mol.%	An	92.9	91.4	89.8	90.8
	Ab	6.9	8.4	9.8	9.0
	Or	0.2	0.2	0.4	0.2

isothermal experiment suggests that, if the melt was cooled at approximately 10°/hr, plagioclase would nucleate at 1110°C (Table 7); i.e. 20° below the equilibrium plagioclase saturation temperature. The small width of the crystals ($<10\,\mu$) makes detection of zoning impractical. The plagioclases are non-stoichiometric to an extent identical with lunar olivine basalt 12063 (Crawford, 1973, Fig. 3a).

Chromite. There is essentially constant core composition ($chr_{40-45}pcr_{12-16}sp_{29-32}uv_{9-12}$) of chromite as a function of cooling rate (Table 8). Chromite clearly nucleates at essentially constant temperature in all runs. The continuous increase in Fe/Fe + Mg ratio from core to rim is small. Narrow mantles of chromian ulvöspinel overgrow the chromites in the log $t \propto T$ run.

Glass. Changes in residual glass composition as a function of cooling rate and isothermal crystallization temperature (Table 9) show systematic variation for each element, best shown by the TiO_2 content and MgO/MgO + FeO ratio. Both parameters initially increase with cooling rate (e.g. TiO_2 in Fig. 7a). The maximum TiO_2 content and MgO/MgO + FeO ratio are in glass from the 15.5°/hr cooling rate run; at slower cooling rates, ilmenite nucleates and both parameters show less extreme changes from the starting composition. The cooling runs were all quenched at approximately 1090°C. If the value of TiO_2 in the residual glass of the cooling rate experiments is compared with that projected for an isothermal crystallization experiment at 1090°C (Fig. 7a,b), then it is seen that the liquid line of descent followed during fractional crystallization under cooling rate conditions is considerably different from the equilibrium liquid line of descent. It is also clear

Table 8. Spinel analyses.

	40°/hr		15°/hr		7°/hr		$T \propto \log t$			Chromite in
	core	rim	core	rim	core	rim	core	rim	ilmenite	sample 12009
TiO_2	3.47	3.46	4.49	4.51	3.61	3.65	3.31	23.58	52.09	4.75
Al_2O_3	15.98	15.99	15.26	14.67	15.40	14.86	15.75	3.74	0.09	12.74
Cr_2O_3	46.47	46.27	46.50	45.53	47.21	46.48	46.41	16.23	0.16	47.39
FeO	22.40	24.30	24.91	29.74	23.53	26.74	23.25	54.13	45.99	25.61
MnO	n.d.	n.d.	n.d.	n.d.	n.d.	n.d.	0.30	0.41	0.39	0.31
MgO	10.38	8.92	9.43	6.03	9.45	7.07	8.59	0.92	0.27	7.55
Total	98.70	98.94	100.59	100.48	99.20	98.80	97.61	99.01	98.99	98.35
Ti	0.678	0.679	0.871	0.895	0.709	0.723	0.661	5.237	0.997	0.959
Al	4.898	4.924	4.635	4.567	4.733	4.616	4.938	1.301	0.003	4.042
Cr	9.553	9.557	9.473	9.508	9.734	9.684	9.759	3.787	0.003	10.090
Fe	4.870	5.308	5.368	6.569	5.131	5.892	5.173	13.375	0.979	5.770
Mn	—	—	—	—	—	—	0.064	0.107	0.008	0.074
Mg	4.021	3.475	3.621	2.372	3.672	2.775	3.402	0.405	0.010	3.029
No. of oxygens	32	32	32	32	32	32	32	32	3	32

Table 9. Glass analyses.

Cooling rate or temperature	1430°/hr	650°/hr	380°/hr	86°/hr	40°/hr	15.5°/hr	7°/hr	1110°C	1150°C	1180°C	1190°C
SiO_2	46.48	45.23	46.98	46.25	48.44	46.79	47.48	44.61	47.70	46.87	47.53
TiO_2	2.74	2.83	3.25	3.21	3.27	5.76	5.04	5.67	3.15	3.09	3.05
Al_2O_3	10.41	10.19	11.61	10.99	12.31	10.09	11.39	10.80	12.27	11.60	11.47
Cr_2O_3	0.39	0.44	0.23	0.43	0.15	0.02	0.04	0.11	0.23	0.26	0.24
FeO	16.59	16.76	15.09	16.42	14.56	21.87	19.15	20.81	14.60	15.23	14.82
MnO	0.28	0.33	0.26	0.27	0.25	0.37	0.35	0.30	0.30	0.26	0.28
MgO	11.36	9.45	7.54	8.13	6.84	3.23	4.22	5.31	7.68	8.49	8.69
CaO	11.79	12.66	13.21	13.46	13.69	10.56	11.03	11.61	13.47	13.38	12.98
Na_2O	0.23	0.23	0.28	0.23	0.32	0.24	0.22	0.32	0.26	0.27	0.29
Total	100.27	98.12	98.45	99.39	99.83	98.93	98.92	99.54	99.66	99.45	99.35
MgO/MgO + FeO wt. ratio	0.41	0.36	0.33	0.33	0.32	0.13	0.18	0.20	0.34	0.36	0.37

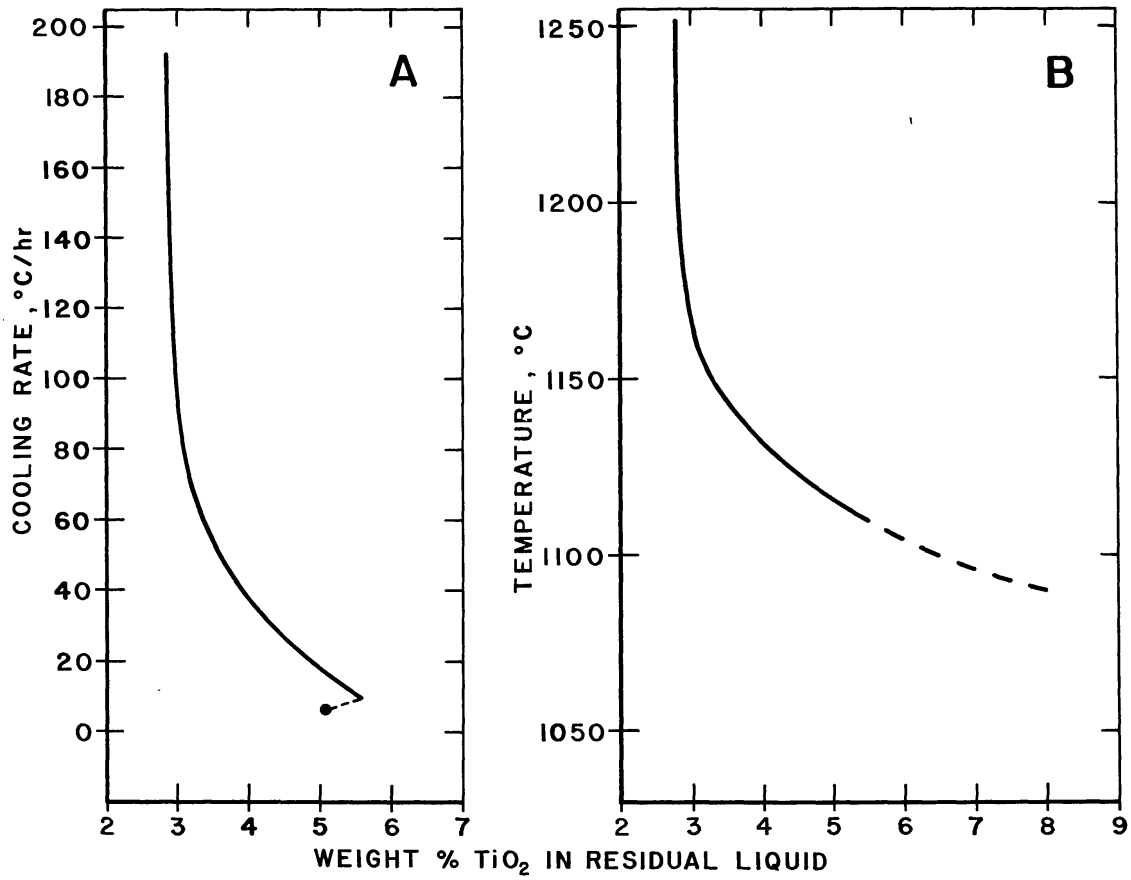

Fig. 7. Variation in TiO_2 content of residual liquid (glasses) in cooling rate runs (a) and isothermal runs (b). All the cooling rate runs were quenched within 10°C of 1090°C. The dashed line in Fig. 7b is an extrapolation to 1090°C, assuming no ilmenite crystallization.

that continuous cooling of the melt suppresses TiO_2 enrichment of the residual glass at a given isotherm and also depresses the solidus temperature. Cooling at 15.5°/hr to 1090°C produces a residual glass with TiO_2 content comparable to that in the 1110°C isothermal run. If TiO_2 content of the residual melt is taken as an index of extent of solidification, then the solidus of this cooling rate run is depressed by 20°C.

Comparison with olivine vitrophyre 12009

The compositions of olivine, pyroxene, and spinel crystals in sample 12009 (thin section numbers 8, 10, and 13) were determined for comparison with the run products obtained in this study (Tables 5, 6, and 8). The most magnesian olivine Fo_{76} (cf. Butler, 1972) is more Fe-rich than that in the experiments, reflecting the lower Mg/Mg + Fe ratio of the rock compared to the analog (Table 2). Olivine crystals of different shapes in the rock (Types I, II, and III; described in a later section) have distinct core compositions, reflecting different nucleation temperatures. Minor-element contents of the natural and synthetic crystals are similar; the systematic increases in Ti and Ca contents from Type I to Type III crystals correspond to an increase in cooling rate (Table 5).

Contrary to the statement of Green *et al.* (1971, p. 605), some of the pyroxenes in sample 12009 have pigeonite cores (Table 6), but these are not present in the experimental runs. This feature, together with the lower Mg/Mg + Fe ratio of the pyroxenes in 12009 (Fig. 4), is due to the differences in bulk composition between the analog and the rock (Table 2). Figures 4 and 5 indicate that only a portion of the fractionation trend of the natural pyroxenes has been reproduced.

The chromite in sample 12009 is of comparable composition to that in the experiments (Table 8), though it is relatively Al- and Mg-poor, in accord with the lower Al content and Mg/Mg + Fe ratio of the rock compared to the analog. Curiously, the chromite is unzoned, in contrast to the crystals in the cooling rate experiments, and presumably grew under essentially isothermal conditions. Ilmenite in sample 12009 is too fine-grained to analyze.

Cooling History of the Olivine Basalt Group

The experiments confirm the conclusion of Lofgren *et al.* (1974) that there are *systematic* changes in the texture, crystal shapes and sizes, mineral and residual glass compositions and mineral zoning trends of igneous rocks as functions of both cooling rate and degree of supercooling. The systematic variations in these properties within suites of mare basalt samples (e.g. Dowty *et al.*, 1974) can also be attributed to differences in cooling rate and degree of supercooling during crystallization of the magma. It should therefore be possible, from comparison of the petrographic features of experiments and of mare basalt samples, to deduce for the natural rocks the cooling rate and the approximate degree of supercooling at which the crystalline phases nucleated. In performing this exercise, it must be assumed that differences in bulk composition between the natural rocks, and between the rocks and the synthetic analog of 12009, do not greatly affect the rock texture. (See additional comments in penultimate section.) The values of cooling rate assigned to the Apollo 12 rocks in this study are believed to be within a factor of 3 of the real values.

1. *Olivine vitrophyre* 12009

Sample 12009 contains three shapes of olivine crystals (Types I, II, and III in Table 5):

(I) Glomerocrysts of subhedral crystals (homogeneous cores of $Fo_{75.1–75.8}$ and narrow mantles zoned from $Fo_{70–54}$), some with chain-like overgrowths on edges and corners (Fig. 8a).

(II) Large, single, subequant skeletons (homogeneous cores of $Fo_{69.6–70.9}$ and narrow mantles zoned to Fo_{54}) with essentially euhedral outline, but internal skeletal structure resulting from incomplete crystallization of faces of the form {021} (Fig. 8b).

(III) Small, subequant to elongate skeletons, chain-like crystals and occasionally crystals with lattice-work shapes (cores of $Fo_{67–69}$ continuously zoned to Fo_{54}; Fig. 8c).

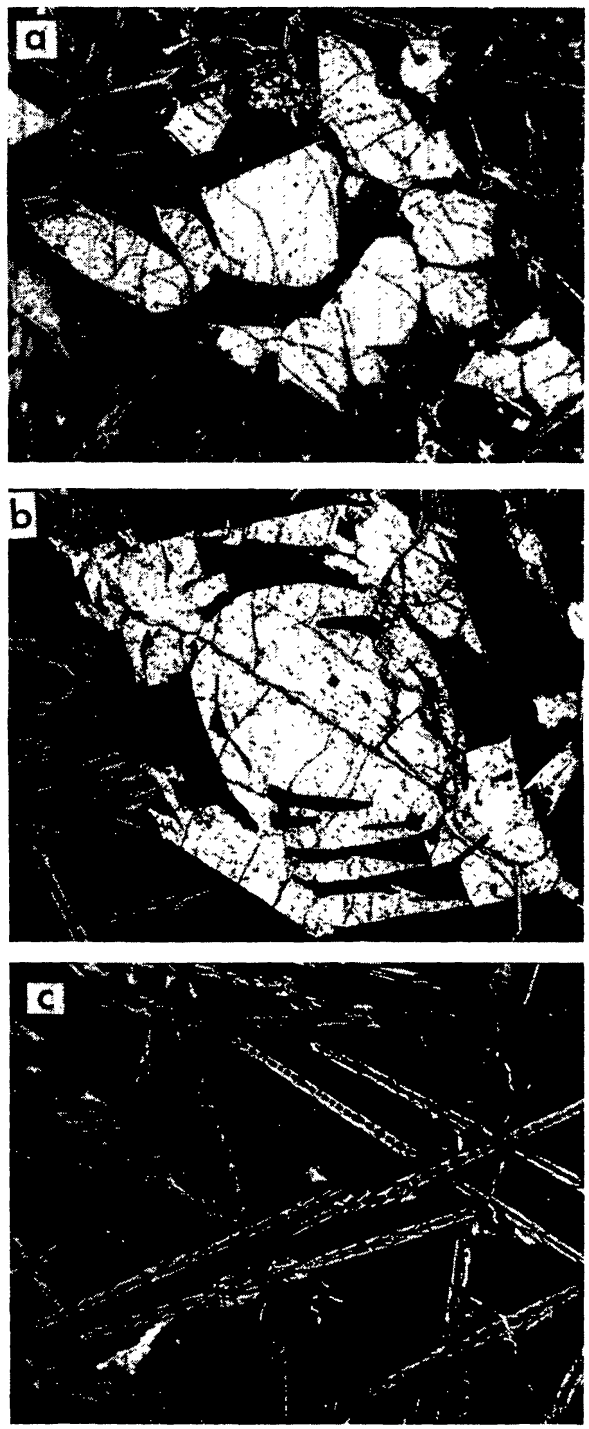

Fig. 8. The different shapes and sizes of olivine crystals in olivine vitrophyre 12009. Field of view in brackets. (a) Type I olivine (2.2 mm); (b) Type II olivine (1.2 mm); (c) Type III olivine (1.2 mm).

Olivine crystals of size and shape comparable to the second variety listed above grow when the analog of 12009 is cooled at 7°/hr (Fig. 2h). Chain-like and lattice-work olivines grow at cooling rates ≥80°/hr (Table 2). Subhedral crystals presumably grow when the melt is cooled at less than 2.7°/hr. These cooling rates indicate the likely values at which each crystal shape grew in a magma of 12009 composition.

In each cooling rate experiment [including the two-stage cooling histories (Table 1a)], only one type of olivine grain size and crystal shape grew, and very large differences in cooling rate (>80°/hr) were found necessary to reproduce the phenocryst and groundmass olivine crystal shapes in olivine vitrophyre 12009. These differences imply that the spectrum of shapes and sizes of olivine crystals in single thin sections of Apollo 12 olivine vitrophyres results from crystallization in at least two thermal regimes, first in a large magma body, and then in a smaller one.

We suggest the following crystallization and emplacement history for sample 12009. The subhedral olivines (Type I crystals) grew as a melt of 12009 composition rose in the lunar crust and cooled slowly from its liquidus temperature at less than 2.7°/hr. (Chromite also crystallized at this time.) Turbulence in a narrow conduit may have caused the synneutic accretion of these crystals into glomerocrysts (Vance, 1969). Following eruption, the magma cooled at a continuously increasing rate (Fig. 9). Initially the rate was less than 10°/hr and large skeletal olivines (Type II crystals) crystallized. As the rate increased to greater than 100°/hr, olivine nucleation rate increased, the skeletal crystals became more

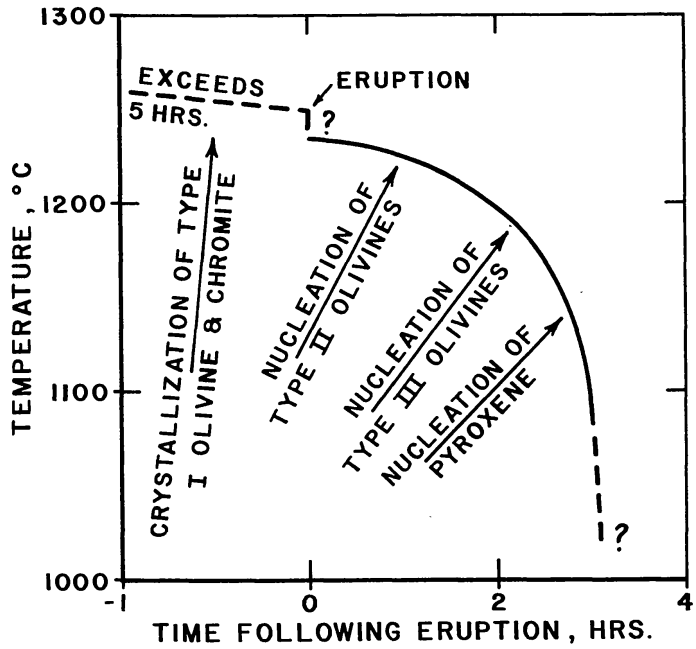

Fig. 9. Suggested cooling path during crystallization of sample 12009, assuming it has the composition of the analog. The curve is constructed from an estimate, based on crystal shape, of the cooling rate at the time of nucleation of each type of olivine crystal and the nucleation temperature (Tables 2 and 3).

elongate and were replaced by chain-like and lattice-work shapes (Type III crystals). Some of these elongate skeletons grew from new crystal nuclei, others grew from corners of the subhedral crystals (Fig. 8). Like experimental runs cooled at 40°/hr and faster, sample 12009 contains no plagioclase, implying that the cooling rate probably exceeded 40°/hr before the temperature reached 1130°C, at which plagioclase crystallizes in equilibrium experiments (Fig. 1).

The distinct difference in core compositions of Type I and Type II olivines agrees with this two-stage cooling model. The overlap in Type II and Type III core compositions and the difference in their Ti and Ca contents (Table 5) confirms that the cooling rate *continuously* increased following eruption. Unfortunately, the difference in composition between sample 12009 and the analog precludes using Fig. 3a and b to determine the cooling rate and nucleation temperature of the three olivine types in the rock.

The curve in Fig. 9 is only an estimate of how sample 12009 cooled. In particular, the temperature drop following eruption is unknown, so that the time at which Type II olivines nucleated is unknown. Nonetheless, it is clear that, following eruption, sample 12009 solidified in only a few hours. The upwardly-convex shape of the cooling curve is consistent with cooling at the center of a flow, whereas the upwardly-concave form of the cooling curve deduced by Walker *et al.* (1975) for sample 12002 suggests derivation of 12002 from the margin of a flow (Lofgren *et al.*, this volume). Since sample 12002 cooled much more slowly than 12009, it might be concluded that sample 12009 crystallized at the center of a much thinner lava flow than sample 12002. However, other explanations are possible for the increasing cooling rate of sample 12009 following eruption; e.g. the sample might be a tongue, or blister, of magma extruded from a lava flow following crystallization of Type II olivine crystals, or the Type II crystals might be transported by turbulence from a site within the flow to the margin. If the groundmass olivine in 12009 is considered to have crystallized at approximately 100°/hr at the center of a cooling unit, the unit is calculated to be approximately 20 cm thick.

In the three runs involving two-stage cooling (slow→fast; Table 1a), only one generation of olivine crystallized. The most likely cause of this failure to reproduce the texture of sample 12009 is that the temperature at which the cooling rate is increased, and hence the normative olivine content of the melt remaining after crystallization of olivine phenocrysts, is critical. The temperature of 1200°C, at which the cooling rate was increased, is probably too low.

The experiments indicate that rapid cooling of a "mafic" melt at low-oxygen fugacity promotes crystallization of olivine at the expense of pyroxene. In very rapidly cooled runs, the amount of modal olivine in a charge may exceed the normative olivine content by as much as 15 vol.%. With progressively slower cooling, the excess of modal olivine relative to normative olivine diminishes. One portion of sample 12009 lacks chain-like and lattice-work olivine, its place being taken by groundmass pyroxene. The experiments indicate that this variation is attributable to a slower rate of cooling (<80°/hr) in the portion containing groundmass pyroxene. This variation in cooling rate suggests movement of magma, even when crystallization was far advanced.

2. *Olivine basalts and gabbros*

Vitrophyres 12009 and 12008 are the most rapidly cooled samples among the Apollo 12 olivine basalt group. Other members of the group lack groundmass olivine and, on eruption, cooled more slowly than 80°/hr. These samples consist of ophitic-textured rocks of differing grain sizes. By comparison with the present experiments, the more finely crystalline *olivine basalts* cooled at rates less than 15°/hr, and the more coarsely crystalline *olivine gabbros* cooled at rates slower than 2.5°/hr. We examined eight olivine basalt group rocks in the Curator's collection and rank them in the following order of decreasing post-eruption cooling rate: 12009 and 12008 → 12075 → 12004 → 12018 → 12020 → 12035 and 12040 (cf. James and Wright, 1972; Table 1).

Origin and Significance of Porphyritic Texture

It is critical to distinguish use of the term "porphyritic" to describe a rock in which one mineral, *not necessarily present in two grain sizes*, is much larger than grains of other minerals [definition of Holmes (1920)], from its use to indicate that two different grain sizes of the *same mineral* are present in a rock [definition of Rosenbusch (1882)]. In many of the Apollo 12 olivine basalts, large olivine crystals (phenocrysts) are set in finer-grained matrices of plagioclase, pyroxene and opaque minerals. The results of this study indicate that this porphyritic texture can develop during linear cooling at rates less than 40°/hr. The causes of formation of the texture—the ease and low rate of olivine nucleation from mafic magmas (Wager, 1959) and the rapid growth rate of olivine in olivine-rich melts (Drever and Johnston, 1957)—are well known.

Porphyritic texture has now been produced experimentally during *linear cooling* of two types of mare basalt (olivine-normative and quartz-normative). There is, however, the notable difference that the two crystal generations of one mineral grown in the quartz-normative basalt (Lofgren *et al.*, 1974) are not found in the olivine basalt. Lofgren and Donaldson (1975) have produced a porphyritic texture during linear cooling of a terrestrial ocean ridge tholeiite, in which plagioclase "phenocrysts" are set in fine-grained pyroxene. A necessary condition for growth of phenocrysts, *under single-stage cooling conditions*, seems to be that the phenocryst phase(s) crystallizes over a wide temperature range (up to 30°C) before appearance of another phase. More specific conditions are necessary for crystallization of a phase in two crystal generations under single-stage cooling conditions (Lofgren *et al.*, 1974).

As indicated in the previous section, the glomerocrysts of olivine in sample 12009 are best regarded as pre-eruption phenocrysts which grew during slower cooling than the groundmass crystals. Hence, prior to eruption, there could have been concentration of olivine (of Type I crystals) and chromite, or loss of them from magma, such that 12009 is not an unfractionated liquid composition. [Green *et al.* (1971) give compelling reasons why accumulation of olivine in 12009, if it occurred at all, was slight, and the presence of <5% of Type I olivines in the rock is in agreement with this conclusion.] Since this is true of the olivine phenocrysts

in the vitrophyres, it may also be true of the olivine phenocrysts in the olivine basalts and gabbros. Hence, although the textural modeling at uniform cooling rates indicates that the *olivine basalts* could have erupted free of crystals, the presence of more than one generation of olivine in the *vitrophyres* suggests that this conclusion is illusory.

INTERLABORATORY COMPARISON

Walker *et al.* (1975) have performed a similar type of study on olivine basalt sample 12002, which is slightly richer in Mg and poorer in Fe than sample 12009 and has a liquidus temperature 70–100°C higher than that of 12009. It is instructive to contrast the results of the two studies of olivine basalt, to caution that different results can be obtained by two laboratories, and to discuss the causes of the differences.

Independent of the cooling rate, Walker *et al.* (1975) found that the core composition of olivine crystals was Fo_{78}. In agreement with this finding, they also observed that in all cooling experiments olivine nucleation took place very close to the liquidus temperature (e.g. cooling at 1000°/hr, nucleation occurred within 20°C of the liquidus). In contrast, olivines grown in this study vary systematically in core composition with cooling rate (Fig. 3b). In a series of experiments cooling at 1000°/hr, the analog of sample 12009 could be supercooled up to 100°C before spontaneous nucleation of olivine. Also, the isothermal supercooling experiments indicate that during cooling (at 2500°/hr) from superliquidus temperatures to a crystallization isotherm, it can take from 5–30 min after reaching the isotherm before olivine nucleates. Clearly, in our experiments the incubation time for olivine nucleation is appreciable at all isotherms, whereas in those of Walker *et al.* (1975) it is negligible. This difference between laboratories may be attributable to the differing experimental techniques. Working with iron as a sample container enclosed in an evacuated silica tube, the charges of Walker *et al.* (1975) are always saturated with iron; i.e. iron is the liquidus phase of the experimental melt. Tentatively, we suggest that the iron in the melt acts as heterogeneous nuclei for olivine, thereby raising the olivine nucleation temperature relative to that for spontaneous nucleation. The work of Walker *et al.* (1975) indicates that the *temperature of heterogeneous nucleation* is essentially unaffected by cooling rate. The melt in the present study is not saturated with iron during olivine nucleation and hence, on cooling, all olivine nucleation must be spontaneous. The results indicate that the *spontaneous nucleation temperature* can be suppressed with increasing cooling rate (cf. Donaldson, 1974). With regard to the liquid line of descent followed by a fractionating mare basalt, this interlaboratory comparison indicates that the manner of olivine nucleation (heterogeneous as opposed to homogeneous or spontaneous) is critical.

Whereas Walker *et al.* (1975) grew two pyroxene generations during linear cooling of the 12002 melt, pyroxene persistently crystallized in only one generation in the linear cooling experiments performed for this study. Also, Walker *et al.*

(1975) find a range of crystal morphologies at each cooling rate investigated, such that only a *gross* estimate of cooling rate (within a few hundred °/hr) can be obtained from crystal shapes. In this study, both olivine and pyroxene crystals generally show one distinct type of morphology in each charge, such that we consider crystal morphology to be a very sensitive index of cooling rate (cf. Lofgren *et al.*, 1975a). In comparing the results of nonequilibrium (cooling rate) experiments from different laboratories, the reader must appreciate that the effects of different oxygen fugacity (Lofgren *et al.*, this volume) and experimental technique (sample mass, sample mass to container mass, container material, surface area of contact between sample and container, shape of melt, degree of superheating and melting duration before cooling) may affect the crystal shapes and textures of the run products. For example, it seems that differences in oxygen fugacity, experimental technique, and possibly melt composition are responsible for the formation of a porphyritic texture, *with two generations of pyroxene*, in linearly cooled melts of Apollo 12 olivine basalt composition. Recent crystallization studies on a terrestrial basalt (Lofgren and Donaldson, 1975) indicate that the composition of the gas phase in contact with the charge markedly affects the nucleation and growth rates of plagioclase, even at constant f_{O_2}. The effect of running in a flowing gas atmosphere, as opposed to a vacuum, may be a significant difference between the present experiments and those of Walker *et al.* (1975).

It is stressed that these factors could cause interlaboratory differences in the crystallization of cooled melts. However, the detail with which the textures, crystal shapes and mineral chemistry of mare basalts have been reproduced (Lofgren *et al.*, 1974; Walker *et al.*, 1975; Usselman *et al.*, 1975; this paper) indicates clearly that experimental crystallization closely resembles natural crystallization. It is details of the results that differ between laboratories, not major results. Thus, the cooling rates of the olivine basalt group deduced by Walker *et al.* (1975) and by us are comparable.

Summary

Following eruption, the Apollo 12 olivine *vitrophyres* cooled at rates which increased from 10°/hr to at least 100°/hr, whereas the *basalts* cooled at rates less than 15°/hr and the *gabbros* at less than 2.7°/hr. The multiple generations of olivine in the vitrophyres indicate that the magmas contained olivine crystals prior to eruption, as may have the olivine basalts and gabbros, which contain one generation of olivine. The textures and crystal morphologies in this type of nonequilibrium experimentation should be interpreted and applied with caution, for they are sensitive to oxygen fugacity, experimental technique and possibly also small changes in melt composition.

Acknowledgments—C. H. Simonds kindly provided the starting material. R. H. Hewins and D. R. Uhlmann suggested many improvements to the manuscript. C. H. Donaldson thanks the Lunar Science Institute for a Visiting Graduate Fellowship and the Natural Environment Research Council (U.K.) for financial support. T. M. Usselman is supported by a NRC-NASA Resident Research Associateship.

The Lunar Science Institute is operated by the Universities Space Research Association under Contract No. NSR 09-051-001 with the National Aeronautics and Space Administration. This paper is the Lunar Science Institute Contribution No. 217. We were inspired by Robert Bruce (and spider), Monty Python, The Alamo, and Guinness.

REFERENCES

Brett R., Butler P., Meyer C., Reid A. M., Takeda H., and Williams R. (1971) Apollo 12 igneous rocks 12004, 12008, 12009 and 12022: A mineralogical and petrological study. *Proc. Lunar Sci. Conf. 2nd*, p. 301–317.

Butler P. (1972) Compositional characteristics of olivines from Apollo 12 samples. *Geochim. Cosmochim. Acta* **36**, 773–785.

Compston W., Berry H., Vernon M. J., Chappell B. W., and Kaye M. J. (1971) Rubidium–strontium chronology and chemistry of lunar material from the Ocean of Storms. *Proc. Lunar Sci. Conf. 2nd*, p. 1471–1485.

Crawford M. L. (1973) Crystallization of plagioclase in mare basalts. *Proc. Lunar Sci. Conf. 4th*, p. 705–717.

Donaldson C. H. (1974) Olivine crystal types in harrisitic rocks of the Rhum pluton and in Archean spinifex rocks. *Geol. Soc. America Bull.* **85**, 1721–1726.

Donaldson C. H., Williams R. J., and Lofgren G. E. (1975) A sample holding technique for study of crystal growth in silicate melts. *Amer. Mineral.* **60**, 324–326.

Dowty E., Keil K., and Prinz M. (1974) Lunar pyroxene–phyric basalts: Crystallization under supercooled conditions. *J. Petrol.* **15**, 419–453.

Drever H. I. and Johnston R. (1957) Crystal growth of forsteritic olivine in magmas and melts. *Trans. Roy. Soc. Edin.* **63**, 289–315.

Drever H. I., Johnston R., Butler P., and Gibb F. G. F. (1972) Some textures in Apollo 12 lunar igneous rocks and in some terrestrial analogs. *Proc. Lunar Sci. Conf. 3rd*, p. 171–184.

Gibb F. G. F. (1974) Supercooling and the crystallization of plagioclase from a basaltic magma. *Mineral. Mag.* **39**, 641–653.

Green D. H., Ringwood A. E., Ware N. G., Hibberson W. O., Major A., and Kiss E. (1971) Experimental petrology and petrogenesis of Apollo 12 basalts. *Proc. Lunar Sci. Conf. 2nd*, p. 601–615.

Holmes A. (1920) *The Nomenclature of Petrology*. New York.

Hopper R. W. and Uhlmann D. R. (1974) Solute redistribution during crystallization at constant velocity and constant temperature. *J. Crys. Growth* **21**, 203–213.

James O. B. and Wright T. L. (1972) Apollo 11 and 12 mare basalts and gabbros: Classification, compositional variations, and possible petrogenetic relations. *Geol. Soc. America Bull.* **83**, 2357–2382.

Lofgren G. E. and Donaldson C. H. (1975) Phase relations and non-equilibrium crystallization of ocean ridge tholeiite from the Nazca Plate (abstract). *EOS* (*Trans. Amer. Geophys. Union*) **56**, 468.

Lofgren G. E., Donaldson C. H., Williams R. J., Mullins O., and Usselman T. M. (1974) Experimentally reproduced textures and mineral chemistry of Apollo 15 quartz normative basalts. *Proc. Lunar Sci. Conf. 5th*, p. 549–568.

Lofgren G. E., Usselman T. M., and Donaldson C. H. (1975) Cooling history of Apollo 15 quartz normative basalts determined from cooling rate experiments (abstract). In *Lunar Science VI*, p. 515–517. The Lunar Science Institute, Houston.

Lofgren G. E., Usselman T. M., and Donaldson C. H. Geology, petrology and crystallization of Apollo 15 quartz normative basalts. *Proc. Lunar Sci. Conf. 6th*. This volume.

Rosenbusch H. (1882) Veber das wesen der Körnigen und porphyrischen structur bei massengesteinen. *Neus Jahrb.* **2**, 13–14.

Sato M., Hickling N. L., and McLane J. E. (1973) Oxygen fugacity values of Apollo 12, 14 and 15 lunar samples and reduced state of lunar magmas. *Proc. Lunar Sci. Conf. 4th*, p. 1061–1079.

Usselman T. M., Lofgren G. E., and Donaldson C. H. (1975) Experimentally reproduced textures and mineral chemistries of high titanium mare basalts. *Proc. Lunar Sci. Conf. 6th.* This volume.

Vance J. A. (1969) On Synneusis. *Contrib. Mineral. Petrol.* **24**, 7–29.

Wager L. R. (1959) Differing powers of crystal nucleation as a factor producing diversity in layered igneous intrusions. *Geol. Mag.* **96**, 75–80.

Walker D., Kirkpatrick R. J., Longhi J., and Hays J. F. (1975) Crystallization history and origin of lunar picritic basalt 12002: Phase equilibria, cooling rate studies, and physical properties of the parent magma. *Geol. Soc. America Bull.*

Warner J. L. (1971) Lunar crystalline rocks: Petrology and geology. *Proc. Lunar Sci. Conf. 2nd*, p. 469–480.